J Elast (2017) 127:235–247
DOI 10.1007/s10659-016-9611-4

Elastocapillary Coiling of an Elastic Rod Inside a Drop

Hervé Elettro[1] · Paul Grandgeorge[1] · Sébastien Neukirch[1]

Received: 25 January 2016 / Published online: 7 December 2016

Abstract Capillary forces acting at the surface of a liquid drop can be strong enough to deform small objects and recent studies have provided several examples of elastic instabilities induced by surface tension. We present such an example where a liquid drop sits on a straight fiber, and we show that the liquid attracts the fiber which thereby coils inside the drop. We derive the equilibrium equations for the system, compute bifurcation curves, and show the packed fiber may adopt several possible configurations inside the drop. We use the energy of the system to discriminate between the different configurations and find a intermittent regime between two-dimensional and three-dimensional solutions as more and more fiber is driven inside the drop.

Keywords Capillarity · Bifurcation · Packing

Mathematics Subject Classification 74K10 · 74F10 · 74G65

1 Introduction

The packaging of elastic filaments in cavities [27] is a model system for a large variety of physical phenomena, for example the ejection of DNA from viral capsids [16, 18, 19], carbone nanotubes compaction [6], or the windlass mechanism in spider capture threads [30]. In the case of a mechanical wire spooled in a sphere, or DNA in a capsid, the presence of a motor is necessary for the packing process, the energy to bend the filament being provided by this external actuator. In the case the cavity is a liquid drop (or a bubble in a liquid medium) surface tension may provide the actuation energy: if the affinity of the filament for the liquid is stronger than that of the filament for the surrounding gas, then the bending energy required for packing could be provided by the difference of surface energies. As always, surface energy prevails at small scale and carbon nanotubes adopting ring

✉ S. Neukirch
sebastien.neukirch@upmc.fr

[1] Institut Jean Le Rond d'Alembert, Sorbonne Universités, UPMC Univ. Paris 06, CNRS, UMR 7190, 75005 Paris, France

shapes in cavitation bubbles have been experimentally observed [21] and theoretically analyzed [7]. For larger drop-on-fiber systems [11, 20], typically of millimeter or centimeter sizes, the competition between capillary and elastic forces is not automatically won by the former: a threshold length emerges [7] and separates systems in which packaging is possible from those in which the fiber remains straight. This threshold length, called elastocapillary length [25], plays a central role in problems in which surface tension bends or buckles slender rods [15] or thin elastic sheets [24].

Computations of configurations of a filament packaged in a spherical cavity have been performed using Finite Elements [29], molecular mechanics [3], or statistical physics [1] approaches. Here we present a model for the buckling and coiling of an elastic rod in a rigid spherical cavity. In Sect. 3 we derive the equilibrium equations for the elastic rod using an energy approach [5, 26]. In Sect. 4 we non-dimensionalize the equations and set the boundary-value problem which we numerically solve. In Sect. 5 we plot bifurcation curves and compare the energies of the different coiling solutions. We finally present experimental configurations of coiled systems involving elastomeric beams and oil droplets.

2 Surface Tension and Interface Energy

In this section we recall the link between surface tension and surface energy. Any interface between two mediums costs energy as molecules lying at the interface are in a less favorable state than molecules deeply buried in the medium. Theses molecules at the interface are then slightly scattered and therefore in a state of tension: surface energy yields surface tension [8]. We illustrate this link in Fig. 1 which shows a drop sitting on a wall in the absence of gravity. A cylindrical rigid rod is then partially immersed in the liquid drop. The rod's material has a stronger affinity with the liquid than with air and consequently the rod is attracted toward the liquid. One has then to pull the rod at its right end to equilibrate the system. We compute this pulling tension T by writing the potential energy of the system. The solid-liquid interface has energy γ_{SL} per unit area, yielding a total surface energy $\ell_{\mathrm{in}} P \gamma_{\mathrm{SL}} + \Sigma \gamma_{\mathrm{SL}}$ where P is the perimeter and Σ the area of the cylinder cross-section, and ℓ_{in} the immersed length. Similarly the total surface energy of the emerged part (of length ℓ_{out}) is $\ell_{\mathrm{out}} P \gamma_{\mathrm{SV}} + \Sigma \gamma_{\mathrm{SV}}$. The liquid-vapor surface energy is $2\pi R^2 \gamma_{\mathrm{LV}}$ where R is the (constant) radius of the liquid

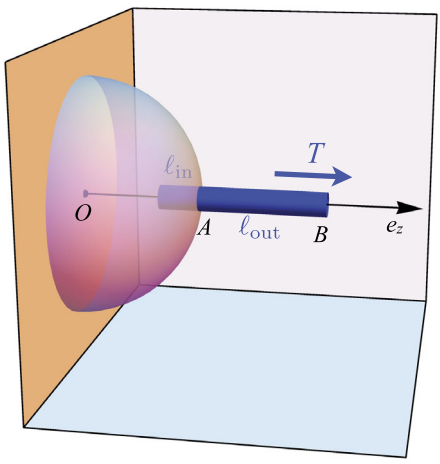

Fig. 1 A cylindrical rigid rod partially immersed in a liquid drop. As affinity of the rod for the liquid is stronger than that with air, a tension T is applied to prevent complete immersion. A capillary force, applied by the liquid at point A, is balancing this tension T

drop. Summing up all these energies, adding the work $-Tz(B)$ of the external tension T, and dropping out constant terms, we write the total potential energy of the system as

$$E = \ell_{\text{in}} P\gamma_{\text{SL}} + \ell_{\text{out}} P\gamma_{\text{SV}} - Tz(B). \tag{1}$$

Replacing $\ell_{\text{in}} = L - \ell_{\text{out}}$ and $z(B) = R + \ell_{\text{out}}$ we finally arrive at

$$E(\ell_{\text{out}}) = \ell_{\text{out}}\big(P[\gamma_{\text{SV}} - \gamma_{\text{SL}}] - T\big) + \text{const.} \tag{2}$$

Equilibrium is then achieved for $\mathrm{d}E/\mathrm{d}\ell_{\text{out}} = 0$ that is

$$T = P(\gamma_{\text{SV}} - \gamma_{\text{SL}}) > 0. \tag{3}$$

In the language of forces we say that the external tension T is balanced by a capillary force $F_\gamma = P(\gamma_{\text{SV}} - \gamma_{\text{SL}})$, applied by the liquid on the rod at point A and oriented toward the center of the drop.

3 Variational Approach

We consider a rod that is naturally straight and has a linear elastic response to bending and twisting. In addition, we work under the assumption that the rod is inextensible and unshearable. The position of the center line of the rod is $\mathbf{R}(S)$ where S is the arc length along the rod. The arc length runs from 0 to L, L being the total contour length of the rod. To follow the deformation of the rod material around the center line, we use a set of Cosserat orthonormal directors $\{\mathbf{d}_1(S), \mathbf{d}_2(S), \mathbf{d}_3(S)\}$ where $\mathbf{d}_3(S)$ is the tangent to the rod center line and $\{\mathbf{d}_1(S), \mathbf{d}_2(S)\}$ register the rotation of the rod cross section about the tangent. Orthonormality of the Cosserat frame implies the existence of a Darboux vector $\mathbf{U}(S)$ such that

$$\mathbf{d}_i'(S) = \mathbf{U}(S) \times \mathbf{d}_i(S), \quad i = 1, 2, 3. \tag{4}$$

The components $U_i = \mathbf{U} \cdot \mathbf{d}_i$ are used to write the strain energy of the rod

$$E_{\text{strain}} = \int_0^L (1/2)\big[K_1 U_1^2(S) + K_2 U_2^2(S) + K_3 U_3^2(S)\big]\mathrm{d}S, \tag{5}$$

where K_1 and K_2 are the bending rigidities, K_3 is the twist rigidity, U_1 and U_2 are the curvature strains, and U_3 is the twist strain [2, 4].

A liquid drop of mass M and radius R is attached to the rod, see Fig. 2. The rod enters the drop at meniscus point A and exits the drop at meniscus point B. Writing S_A the arc length of point A and S_B the arc length of point B, we divide the rod in three regions: (I) where $S \in [0; S_A)$, (II) where $S \in (S_A; S_B)$, and (III) where $S \in (S_B; L]$, with region (II) lying inside the liquid drop. In regions (I) and (III) the solid-vapor interface has an energy γ_{SV} per unit area. In region (II) the solid-liquid interface has energy γ_{SL} per unit area. The total surface energy of the rod then scales linearly with the contour length:

$$E_{\text{surface}} = P\big[\gamma_{\text{SV}} S_A + \gamma_{\text{SL}}(S_B - S_A) + \gamma_{\text{SV}}(L - S_B)\big], \tag{6}$$

where P is the perimeter of the cross-section of the rod. If the drop was free-standing it would adopt a spherical shape in order to minimize its surface energy. Nevertheless due to

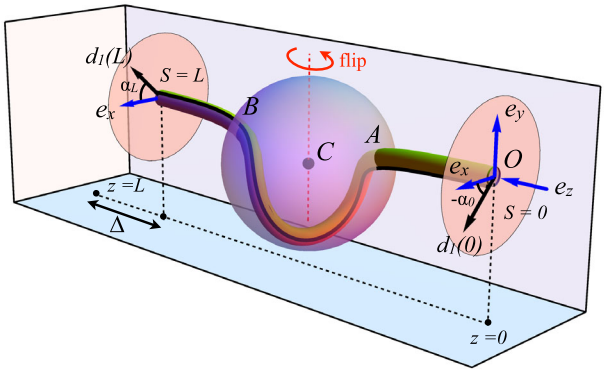

Fig. 2 Equilibrium configuration of an elastic rod buckled by a liquid spherical drop. The rod is clamped at both extremities, and an end-shortening Δ is imposed. The configuration is symmetric about a π-rotation about the axis joining the center C of the sphere and the rod middle point $S = L/2$. Meniscus forces, applied on the rod at meniscus points A and B, together with soft-wall barrier forces are represented. Their sum is equal to the weight of the drop, see Eq. (22)

(i) its own weight, (ii) contact pressure coming from the coiled rod, and (iii) meniscus contact angles, the drop is non-spherical. But as we deal with (i) drops which are smaller than the capillary length, (ii) rods which are flexible compared to surface tension, and (iii) drops with radii much larger than the diameter of the cross-section of the rod, to a first approximation we consider the drop to be spherical. The surface energy $4\pi R^2\gamma_{\mathrm{LV}}$ corresponding to the liquid-vapor interface (*i.e.*, the drop surface) is then constant and therefore discarded. As in [12] we use a soft-wall potential to prevent the rod from exiting the sphere elsewhere than at the meniscus points A and B:

$$V_{\mathrm{wall}}\big(\mathbf{R}(S), \mathbf{R}_C\big) = \frac{V_0}{1 + \rho - (1/R)\sqrt{(\mathbf{R}(S) - \mathbf{R}_C)^2}}, \tag{7}$$

where $\mathbf{R}_C = (X_C, Y_C, Z_C)^T$ is the position of the center of the spherical drop, and V_0 is an energy per unit length with $V_0 \to 0$ corresponding to the hard-wall limit. The small dimensionless parameter ρ is introduced to avoid the potential to diverge at the meniscus points A and B, where the rod enters and exits the sphere. As we are working with sub-millimetric systems we neglect the weight of the rod, but take into account the weight of the drop by adding the term MgY_C into the energy. The total potential energy of the system is then, up to constant terms,

$$E_{\mathrm{tot}} = E_{\mathrm{strain}} + \int_{S_A}^{S_B} V_{\mathrm{wall}} \mathrm{d}S - F_\gamma (S_B - S_A) + MgY_C, \tag{8}$$

where we have introduced the surface tension force $F_\gamma = P(\gamma_{\mathrm{SV}} - \gamma_{\mathrm{SL}}) > 0$. We consider boundary conditions of clamping, where the rod position $\mathbf{R}(S)$ and rotation are restrained at both sides:

$$\mathbf{R}(0) = \mathbf{0}, \qquad \mathbf{R}(L) = (0, 0, L - \Delta)^T, \tag{9a}$$

$$\mathbf{d}_1(0) = \cos\alpha_0 \mathbf{e}_x + \sin\alpha_0 \mathbf{e}_y, \qquad \mathbf{d}_2(0) = -\sin\alpha_0 \mathbf{e}_x + \cos\alpha_0 \mathbf{e}_y, \qquad \mathbf{d}_3(0) = \mathbf{e}_z, \tag{9b}$$

$$\mathbf{d}_1(L) = \cos\alpha_L \mathbf{e}_x + \sin\alpha_L \mathbf{e}_y, \qquad \mathbf{d}_2(L) = -\sin\alpha_L \mathbf{e}_x + \cos\alpha_L \mathbf{e}_y, \qquad \mathbf{d}_3(L) = \mathbf{e}_z, \tag{9c}$$

where Δ is the prescribed end-shortening, α_0 and α_L are fixed angles, and $\{\mathbf{e}_x, \mathbf{e}_y, \mathbf{e}_z\}$ is our reference frame. We minimize E_{tot} under the following constraints

$$\mathbf{R}'(S) = \mathbf{d}_3(S) \quad \text{(inextensibility)}, \tag{10a}$$

$$\mathbf{d}_i(S) \cdot \mathbf{d}_j(S) = \delta_{ij} \quad \text{(orthonormality)}, \tag{10b}$$

$$U_1 = \mathbf{d}_2' \cdot \mathbf{d}_3, \qquad U_2 = \mathbf{d}_3' \cdot \mathbf{d}_1, \qquad U_3 = \mathbf{d}_1' \cdot \mathbf{d}_2 \quad \text{(Darboux relations)}, \tag{10c}$$

$$\big(\mathbf{R}(S_A) - \mathbf{R}_C\big)^2 = R^2 = \big(\mathbf{R}(S_B) - \mathbf{R}_C\big)^2 \quad \text{(position of meniscus)}, \tag{10d}$$

where $' \equiv \mathrm{d}/\mathrm{d}s$. We cope with constraints by introducing Lagrange multipliers and considering the Lagrangian

$$\begin{aligned}
&\mathcal{L}(U_1, U_2, U_3, \mathbf{R}, \mathbf{d}_1, \mathbf{d}_2, \mathbf{d}_3, S_A, S_B, \mathbf{R}_C) \\
&= \int_0^L \big[(1/2)\big(K_1 U_1^2 + K_2 U_2^2 + K_3 U_3^2\big) - M_1\big(U_1 - \mathbf{d}_2' \cdot \mathbf{d}_3\big) - M_2\big(U_2 - \mathbf{d}_3' \cdot \mathbf{d}_1\big) \\
&\quad - M_3\big(U_3 - \mathbf{d}_1' \cdot \mathbf{d}_2\big) - \nu_{12}(\mathbf{d}_1 \cdot \mathbf{d}_2) - \nu_{13}(\mathbf{d}_1 \cdot \mathbf{d}_3) - \nu_{23}(\mathbf{d}_2 \cdot \mathbf{d}_3) \\
&\quad - (1/2)\epsilon_1(\mathbf{d}_1 \cdot \mathbf{d}_1 - 1) - (1/2)\epsilon_2(\mathbf{d}_2 \cdot \mathbf{d}_2 - 1) - (1/2)\epsilon_3(\mathbf{d}_3 \cdot \mathbf{d}_3 - 1)\big]\mathrm{d}S \\
&\quad + (F_A/2R)\big[\big(\mathbf{R}(S_A) - \mathbf{R}_C\big)^2 - R^2\big] + (F_B/2R)\big[\big(\mathbf{R}(S_B) - \mathbf{R}_C\big)^2 - R^2\big] \\
&\quad - F_\gamma(S_B - S_A) - \mathbf{W} \cdot \mathbf{R}_C + \int_{S_A}^{S_B} V_{\text{wall}}\mathrm{d}S \\
&\quad + \int_0^{S_A} \mathbf{N}^{\mathrm{I}} \cdot \big(\mathbf{R}' - \mathbf{d}_3\big)\mathrm{d}S + \int_{S_A}^{S_B} \mathbf{N}^{\mathrm{II}} \cdot \big(\mathbf{R}' - \mathbf{d}_3\big)\mathrm{d}S + \int_{S_B}^{L} \mathbf{N}^{\mathrm{III}} \cdot \big(\mathbf{R}' - \mathbf{d}_3\big)\mathrm{d}S,
\end{aligned} \tag{11}$$

where $\mathbf{W} = (0, -Mg, 0)^T$ is the weight of the drop, and where $M_i(S)$, $\nu_{ij}(S)$, $\epsilon_i(S)$, $\mathbf{N}^{\mathrm{I,II,III}}(S)$, and $F_{A,B}$ are Lagrange multipliers. As we will see in the following, the multipliers $M_i(S)$ correspond to the components of the internal moment $\mathbf{M}$, $\mathbf{M} = M_1\mathbf{d}_1 + M_2\mathbf{d}_2 + M_3\mathbf{d}_3$. It can be shown that, as in the planar case [12], $\mathbf{M}(S)$ does not experience any discontinuity at the meniscus points $S = S_A$ and $S = S_B$. In the same manner, the multipliers $\mathbf{N}^{\mathrm{I,II,III}}(S)$ will be interpreted as the internal force in each region of the system. Since the internal force in the rod does experience discontinuities at the meniscus points, we have therefore introduced three different multipliers $\mathbf{N}^{\mathrm{I,II,III}}(S)$.

First Variation We note $\mathbf{w} = (U_1, U_2, U_3, \mathbf{R}, \mathbf{d}_1, \mathbf{d}_2, \mathbf{d}_3, S_A, S_B, \mathbf{R}_C)$ and we consider the conditions for a state $\mathbf{w}_e$ to minimize the energy E_{tot}. Calculus of variations shows that a necessary condition is

$$\mathcal{L}'(\mathbf{w}_e) \cdot \overline{\mathbf{w}} = \frac{\mathrm{d}}{\mathrm{d}\epsilon}\mathcal{L}(\mathbf{w}_e + \epsilon\overline{\mathbf{w}})|_{\epsilon=0} = 0 \quad \forall \overline{\mathbf{w}}, \tag{12}$$

where $\overline{\mathbf{w}}$ is a variation of the variable $\mathbf{w}$. Boundary conditions (9a)–(9c) imply that

$$\overline{\mathbf{R}}(0) = \mathbf{0}, \qquad \overline{\mathbf{R}}(L) = \mathbf{0}, \tag{13}$$

$$\overline{\mathbf{d}_i}(0, L) = \mathbf{0}, \qquad \overline{\mathbf{d}_i}(L) = \mathbf{0} \quad \forall i. \tag{14}$$

Noting that $\frac{\mathrm{d}}{\mathrm{d}\epsilon}\int_0^{a+\epsilon\overline{a}} f(x)\mathrm{d}x|_{\epsilon=0} = \overline{a}\,f(a)$ we calculate the first variation (12)

$$\begin{aligned}
\mathcal{L}'(\mathbf{w}_e)\cdot\overline{\mathbf{w}} = \int_0^L \big[& K_1U_1\overline{U}_1 + K_2U_2\overline{U}_2 + K_3U_3\overline{U}_3 \\
& - M_1\big(\overline{U_1} - \overline{\mathbf{d}_2}'\cdot\mathbf{d}_3 - \mathbf{d}_2'\cdot\overline{\mathbf{d}_3}\big) - M_2\big(\overline{U_2} - \overline{\mathbf{d}_3}'\cdot\mathbf{d}_1 - \mathbf{d}_3'\cdot\overline{\mathbf{d}_1}\big) \\
& - M_3\big(\overline{U_3} - \overline{\mathbf{d}_1}'\cdot\mathbf{d}_2 - \mathbf{d}_1'\cdot\overline{\mathbf{d}_2}\big) - \nu_{12}(\overline{\mathbf{d}_1}\cdot\mathbf{d}_2 + \mathbf{d}_1\cdot\overline{\mathbf{d}_2}) \\
& - \nu_{13}(\overline{\mathbf{d}_1}\cdot\mathbf{d}_3 + \mathbf{d}_1\cdot\overline{\mathbf{d}_3}) - \nu_{23}(\overline{\mathbf{d}_2}\cdot\mathbf{d}_3 + \mathbf{d}_2\cdot\overline{\mathbf{d}_3}) \\
& - \epsilon_1\overline{\mathbf{d}_1}\cdot\mathbf{d}_1 - \epsilon_2\overline{\mathbf{d}_2}\cdot\mathbf{d}_2 - \epsilon_3\overline{\mathbf{d}_3}\cdot\mathbf{d}_3\big]\mathrm{d}S \\
& + (F_A/R)\big[\big(\mathbf{R}(S_A) - \mathbf{R}_C\big)\cdot\big(\overline{\mathbf{R}}(S_A) + \overline{S_A}\mathbf{R}'(S_A) - \overline{\mathbf{R}_C}\big)\big] \\
& + (F_B/R)\big[\big(\mathbf{R}(S_B) - \mathbf{R}_C\big)\cdot\big(\overline{\mathbf{R}}(S_B) + \overline{S_B}\mathbf{R}'(S_B) - \overline{\mathbf{R}_C}\big)\big] \\
& - F_\gamma(\overline{S_B} - \overline{S_A}) - \mathbf{W}\cdot\overline{\mathbf{R}_C} \\
& + \int_{S_A}^{S_B}\left(\frac{\partial V_{\text{wall}}}{\partial\mathbf{R}}\cdot\overline{\mathbf{R}} + \frac{\partial V_{\text{wall}}}{\partial\mathbf{R}_C}\cdot\overline{\mathbf{R}_C}\right)\mathrm{d}S + \overline{S_B}V_{\text{wall}}(S_B) - \overline{S_A}V_{\text{wall}}(S_A) \\
& + \int_0^{S_A}\mathbf{N}^{\mathrm{I}}\cdot\big(\overline{\mathbf{R}}' - \overline{\mathbf{d}_3}\big)\mathrm{d}S + \int_{S_A}^{S_B}\mathbf{N}^{\mathrm{II}}\cdot\big(\overline{\mathbf{R}}' - \overline{\mathbf{d}_3}\big)\mathrm{d}S + \int_{S_B}^{L}\mathbf{N}^{\mathrm{III}}\cdot\big(\overline{\mathbf{R}}' - \overline{\mathbf{d}_3}\big)\mathrm{d}S.
\end{aligned} \tag{15}$$

Note that we have used (10a) to eliminate several terms. We first require (15) to vanish for all $\overline{U_i}$ and obtain

$$M_i = K_iU_i. \tag{16}$$

Equation (16) appears as the bending/twisting constitutive relation of the elastic rod provided the Lagrange multipliers M_i are seen as the components of the internal moment. We next perform integrations by part for the terms involving $\overline{\mathbf{d}_i}'$. Boundary conditions (14) implies that the boundary terms vanish. Requiring the result to vanish for all $\overline{\mathbf{d}_i}$ yields:

$$M_2\mathbf{d}_3' - M_3'\mathbf{d}_2 - M_3\mathbf{d}_2' - \nu_{12}\mathbf{d}_2 - \nu_{13}\mathbf{d}_3 - \epsilon_1\mathbf{d}_1 = \mathbf{0}, \tag{17a}$$

$$M_3\mathbf{d}_1' - M_1'\mathbf{d}_3 - M_1\mathbf{d}_3' - \nu_{23}\mathbf{d}_3 - \nu_{12}\mathbf{d}_1 - \epsilon_2\mathbf{d}_2 = \mathbf{0}, \tag{17b}$$

$$-\mathbf{N}^{\mathrm{I,II,III}} + M_1\mathbf{d}_2' - M_2'\mathbf{d}_1 - M_2\mathbf{d}_1' - \nu_{13}\mathbf{d}_1 - \nu_{23}\mathbf{d}_2 - \epsilon_3\mathbf{d}_3 = \mathbf{0}. \tag{17c}$$

We take the scalar product of each of these three equations with $\mathbf{d}_1$, $\mathbf{d}_2$, and $\mathbf{d}_3$ and combine them to eliminate the ν_{ij} and the ϵ_i to finally obtain

$$M_1' = M_2U_3 - M_3U_2 + N_2^{\mathrm{I,II,III}}, \tag{18a}$$

$$M_2' = M_3U_1 - M_1U_3 - N_1^{\mathrm{I,II,III}}, \tag{18b}$$

$$M_3' = M_1U_2 - M_2U_1, \tag{18c}$$

which is the component version of the moment balance equation for the elastic rod, $\mathbf{M}' = \mathbf{N}\times\mathbf{R}'$. The Lagrange multiplier $\mathbf{N}$ is then seen as the internal force in the rod. We now

perform integrations by parts for the terms involving $\overline{\mathbf{R}}'$ and find that

$$(F_A/R)\big(\mathbf{R}(S_A)-\mathbf{R}_C\big)\cdot\overline{\mathbf{R}}(S_A)+(F_B/R)\big(\mathbf{R}(S_B)-\mathbf{R}_C\big)\cdot\overline{\mathbf{R}}(S_B)$$
$$+\int_{S_A}^{S_B}\frac{\partial V_{\text{wall}}}{\partial\mathbf{R}}\cdot\overline{\mathbf{R}}\mathrm{d}S+\big[\mathbf{N}^{\mathrm{I}}\cdot\overline{\mathbf{R}}\big]_0^{S_A}+\big[\mathbf{N}^{\mathrm{II}}\cdot\overline{\mathbf{R}}\big]_{S_A}^{S_B}+\big[\mathbf{N}^{\mathrm{III}}\cdot\overline{\mathbf{R}}\big]_{S_B}^{L}$$
$$-\int_0^{S_A}\mathbf{N}^{\mathrm{I}}(S)'\cdot\overline{\mathbf{R}}\mathrm{d}S-\int_{S_A}^{S_B}\mathbf{N}^{\mathrm{II}}(S)'\cdot\overline{\mathbf{R}}\mathrm{d}S-\int_{S_B}^{L}\mathbf{N}^{\mathrm{III}}(S)'\cdot\overline{\mathbf{R}}\mathrm{d}S=0\quad\forall\overline{\mathbf{R}}. \tag{19}$$

This condition implies the balance equations for the rod:

$$\mathbf{N}^{\mathrm{I}}(S)'=\mathbf{0}\quad\forall S\in[0;S_A), \tag{20a}$$
$$\mathbf{N}^{\mathrm{II}}(S)'-\frac{\partial V_{\text{wall}}}{\partial\mathbf{R}}=\mathbf{0}\quad\forall S\in(S_A;S_B), \tag{20b}$$
$$\mathbf{N}^{\mathrm{III}}(S)'=\mathbf{0}\quad\forall S\in(S_B;L], \tag{20c}$$

where $\mathbf{N}^{\mathrm{I,II,III}}$ are the internal forces in each region of the system. The force per unit length $-\partial V_{\text{wall}}/\partial\mathbf{R}$ corresponds to the soft-wall repulsion, from the drop interface, on the rod. Boundary conditions (13) make the boundary terms at $S=0$ and $S=L$ vanish, but arbitrariness of the variations $\overline{\mathbf{R}}(S_A)$ and $\overline{\mathbf{R}}(S_B)$ require that

$$\mathbf{N}^{\mathrm{II}}(S_A)-\mathbf{N}^{\mathrm{I}}(S_A)+F_A\big[\mathbf{R}_C-\mathbf{R}(S_A)\big]/R=\mathbf{0}, \tag{21a}$$
$$\mathbf{N}^{\mathrm{III}}(S_B)-\mathbf{N}^{\mathrm{II}}(S_B)+F_B\big[\mathbf{R}_C-\mathbf{R}(S_B)\big]/R=\mathbf{0}. \tag{21b}$$

These equations correspond to forces balance at the meniscus points. We see that at meniscus points A and B, the total force from the drop on the rod is oriented toward *the center of the spherical drop* and has intensity F_A and F_B respectively. Requiring (15) to vanish for all $\overline{\mathbf{R}_C}$ yields

$$F_A\big[\mathbf{R}_C-\mathbf{R}(S_A)\big]/R+F_B\big[\mathbf{R}_C-\mathbf{R}(S_B)\big]/R=\mathbf{W}+\int_{S_A}^{S_B}\partial V_{\text{wall}}/\partial\mathbf{R}\mathrm{d}S, \tag{22}$$

where we have used the identity $\partial V_{\text{wall}}/\partial\mathbf{R}_C=-\partial V_{\text{wall}}/\partial\mathbf{R}$. Equation (22) tells us that the total meniscus force from the drop on the rod (the right hand side of (22)) is equal to the weight $\mathbf{W}$ of the drop plus the opposite of the integrated soft-wall repulsion. We therefore see that the soft-wall repulsion applied inside the drop is balanced by the meniscus force. Accordingly, using (20b), (21a), (21b), and (22) we find

$$\mathbf{N}^{\mathrm{III}}(S_B)-\mathbf{N}^{\mathrm{I}}(S_A)+\mathbf{W}=\mathbf{0}. \tag{23}$$

That is, the total force from the liquid on regions I and III of the rod is simply the weight of the drop. Finally the conditions for (15) to vanish for all $\overline{S_A}$ and $\overline{S_B}$ are

$$(F_A/R)\big[\mathbf{R}_C-\mathbf{R}(S_A)\big]\cdot\mathbf{R}'(S_A)=F_\gamma-V_{\text{wall}}(S_A), \tag{24a}$$
$$(F_B/R)\big[\mathbf{R}_C-\mathbf{R}(S_B)\big]\cdot\mathbf{R}'(S_B)=-F_\gamma+V_{\text{wall}}(S_B). \tag{24b}$$

These conditions can be seen as a way to compute the intensity F_A and F_B of the meniscus force. In particular we see that F_A (F_B) depends on the relative orientation of the rod's

tangent and the radial vector at the meniscus points A (B), as also shown in [23]. Introducing the tension in rod $T(S) := \mathbf{N} \cdot \mathbf{d}_3$ and using (21a), (21b), we find that

$$T^{\mathrm{I}}(S_A) - T^{\mathrm{II}}(S_A) = F_\gamma - V_{\mathrm{wall}}(S_A), \tag{25a}$$

$$T^{\mathrm{III}}(S_B) - T^{\mathrm{II}}(S_B) = F_\gamma - V_{\mathrm{wall}}(S_B), \tag{25b}$$

where we see that, in the limit $V_0 \to 0$, the jump in the rod's tension is equal to the surface tension force F_γ.

4 Boundary Value Problem

We restrict our attention to rods with isotropic bending behavior, $K_1 = K_2 = K_0$, where $\mathbf{U} = \mathbf{M}/K_0 + (1 - K_3/K_0)U_3\mathbf{d}_3$ with $U_3 = (M_x d_{3x} + M_y d_{3y} + M_z d_{3z})/K_3$. In this case (18c) shows that $\mathrm{d}U_3/\mathrm{d}S \equiv 0\ \forall S$, and consequently $\mathbf{U}$ vanishes for the equations [17, 22]. We additionally focus here on the weightless, $\mathbf{W} = \mathbf{0}$, and symmetrical $S_A = L/2 - \Sigma$, $S_B = L/2 + \Sigma$ case. We use the diameter $D = 2R$ of the spherical drop as unit length, and the buckling load K_0/D^2 as unit force, that is we introduce the following dimensionless quantities

$$s = \frac{S - L/2}{D}; \qquad \ell = \frac{L}{D}; \qquad (x, y, z) = \frac{(X, Y, Z - (L - \Delta)/2)}{D}; \tag{26a}$$

$$\sigma = \frac{\Sigma}{D}; \qquad k_3 = \frac{K_3}{K_0}; \qquad \delta = \frac{\Delta}{D}; \qquad \mathbf{u} = \mathbf{U}D; \qquad f_\gamma = \frac{F_\gamma D^2}{K_0}; \tag{26b}$$

$$\mathbf{n} = \frac{\mathbf{N}D^2}{K_0}; \qquad \mathbf{m} = \frac{\mathbf{M}D}{K_0}; \qquad (v, v_0) = \frac{(V_{\mathrm{wall}}, V_0)D^2}{K_0}. \tag{26c}$$

We further restrict the study to equilibrium shapes being invariant by a rotation of angle π about the line passing through the middle point of the rod, $\mathbf{r}(s = 0)$, and directed along the axis $\mathbf{e}_y$. Such configurations are sometimes referred to as flip-symmetric [10]. The quantities $x(s)$, $z(s)$, $d_{1y}(s)$, $d_{2x}(s)$, $d_{2z}(s)$, $d_{3y}(s)$, $m_y(s)$, and $n_y(s)$ are then odd functions of s, while $y(s)$, $d_{1x}(s)$, $d_{1z}(s)$, $d_{2y}(s)$, $d_{3x}(s)$, $d_{3z}(s)$, $m_x(s)$, $m_z(s)$, $n_x(s)$, and $n_z(s)$ are even functions of s. The center of the spherical drop consequently lies on the flip-symmetry axis, that is $x_C = 0$ and $z_C = 0$, and the end-rotation angles are such that $\alpha_0 = -\alpha_L$. Making use of this symmetry, we only integrate the equilibrium equations for $s \in [0, \ell/2]$, which read

$$x'(s) = d_{3x}, \qquad y'(s) = d_{3y}, \qquad z'(s) = d_{3z}, \tag{27a}$$

$$d'_{1x}(s) = d_{1z}m_y - d_{1y}m_z + (1 - k_3)u_3(d_{1z}d_{3y} - d_{1y}d_{3z}), \tag{27b}$$

$$d'_{1y}(s) = d_{1x}m_z - d_{1z}m_x + (1 - k_3)u_3(d_{1x}d_{3z} - d_{1z}d_{3x}), \tag{27c}$$

$$d'_{1z}(s) = d_{1y}m_x - d_{1x}m_y + (1 - k_3)u_3(d_{1y}d_{3x} - d_{1x}d_{3y}), \tag{27d}$$

$$d'_{3x}(s) = d_{3z}m_y - d_{3y}m_z, \qquad d'_{3y}(s) = d_{3x}m_z - d_{3z}m_x, \qquad d'_{3z}(s) = d_{3y}m_x - d_{3x}m_y, \tag{27e}$$

$$m'_x(s) = d_{3z}n_y - d_{3y}n_z, \qquad m'_y(s) = d_{3x}n_z - d_{3z}n_x, \qquad m'_z(s) = d_{3y}n_x - d_{3x}n_y, \tag{27f}$$

$$n'_x(s) = \chi\, \partial v/\partial x + 2 f_B x(\sigma)\mathrm{d}_{s-\sigma}, \tag{27g}$$

$$n_y'(s) = \chi\, \partial v/\partial y + 2 f_B \big[y(\sigma) - y_C\big] \mathrm{d}_{s-\sigma}, \tag{27h}$$

$$n_z'(s) = \chi\, \partial v/\partial z + 2 f_B z(\sigma) \mathrm{d}_{s-\sigma}, \tag{27i}$$

where d_{s-s_0} is the Dirac distribution centered on s_0, and $v = v_0(1 + \rho - 2\sqrt{x^2 + (y - y_C)^2 + z^2})^{-1}$. For $s \in [0; \sigma)$ the rod lies inside the spherical drop and we have $\chi = 1$, otherwise $\chi = 0$. We set $\alpha = 0$ in (9a)–(9c) and consider v_0, ρ, f_γ, ℓ, and k_3 as fixed parameters. We look for equilibrium solutions by integrating (27a)–(27i) with initial conditions

$$x(0) = 0, \qquad y(0) = y_0, \qquad z(0) = 0, \tag{28a}$$

$$d_{3x}(0) = \sin\theta_0, \qquad d_{3y}(0) = 0, \qquad d_{3z}(0) = \cos\theta_0, \tag{28b}$$

$$d_{1x}(0) = \cos\theta_0, \qquad d_{1y}(0) = 0, \qquad d_{1z}(0) = -\sin\theta_0, \tag{28c}$$

$$n_x(0) = n_{x0}, \qquad n_y(0) = 0, \qquad n_z(0) = n_{z0}, \tag{28d}$$

$$m_x(0) = m_{x0}, \qquad m_y(0) = 0, \qquad m_z(0) = m_{z0} \tag{28e}$$

where $y_0, \theta_0, n_{x0}, n_{z0}, m_{x0}, m_{z0}$ along with y_C, f_B, and σ are 9 unknowns which are balanced by the following 8 conditions. We restrict to cases where the director $\mathbf{d}_1$ is aligned with the $\mathbf{e}_x$ axis at both extremities of the rod, that is we set $\alpha_0 = \alpha_L = 0$. Then, using (9a)–(9c), we write 5 boundary conditions for the right extremity of the rod, $s = \ell/2$

$$x(\ell/2) = 0; \qquad y(\ell/2) = 0; \qquad d_{3x}(\ell/2) = 0; \qquad d_{3y}(\ell/2) = 0; \qquad d_{1y}(\ell/2) = 0; \tag{29}$$

At the meniscus point B, we have 3 conditions, adapted from (10d), (23), and (24b)

$$\sqrt{x^2(\sigma) + \big(y(\sigma) - y_C\big)^2 + z^2(\sigma)} = 1/2, \tag{30a}$$

$$n_y(\sigma) = 0, \tag{30b}$$

$$2 f_B \big[-x(\sigma) d_{3x}(\sigma) + \big(y_C - y(\sigma)\big) d_{3y}(\sigma) - z(\sigma) d_{3z}(\sigma)\big] = -f_\gamma + v(\sigma). \tag{30c}$$

The solution set is thus a $9 - 8 = 1$ dimensional manifold and we plot in Sect. 5 different solution paths.

5 Bifurcation Diagram

We numerically solve the boundary-value problem defined in Sect. 4, using either a shooting method or the AUTO collocation method [9]. Pseudo-arc-length continuation then enables us to follow the solutions as parameters are varied. In order to compare present three-dimensional (3D) results with two dimensional (2D) solutions studied in [12], we use the same parameters $k_3 = 0.9$, $\ell = 10$, $f_\gamma = 20$, and $v_0 = 0.02/\ell^2 = 2 \times 10^{-4}$, but reduce ρ to $\rho = 0.1$ thereby bringing the meniscus points closer to the bounding sphere.

We start with a straight configuration subject to a large applied tension $t = \mathbf{n}(\ell/2) \cdot \mathbf{d}_3(\ell/2)$. We define the end rotation $\mathcal{R}$ as the angle between $\mathbf{d}_1(\ell/2)$ and $\mathbf{d}_1(-\ell/2)$, $\mathcal{R} = \alpha_L - \alpha_0 = 2\alpha_L$ and we first restrict to configurations with $\mathcal{R} = 0$. The straight configuration is consequently twistless. (For the present case of clamped-clamped configurations this end-rotation $\mathcal{R}$ is closely related to the topological link Lk, see, *e.g.*, [28].) As the tension t is

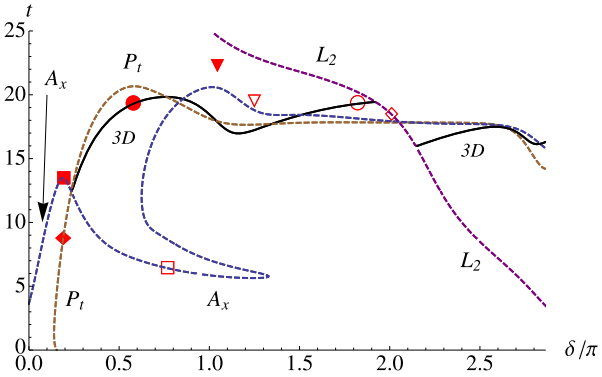

Fig. 3 Force-displacement post-buckling curves for $f_\gamma = 20$ and $\mathcal{R} = 0$, where t is the applied tension and δ the end-shortening. Paths of 3D and 2D configurations are plotted with *solid* and *dashed lines* respectively. Points marked with empty and filled *circles*, *squares*, *diamonds*, and *triangles* correspond to configurations shown in Figs. 5, 6, 7, and 8 respectively. Points marked *triangles* belong to paths not shown here

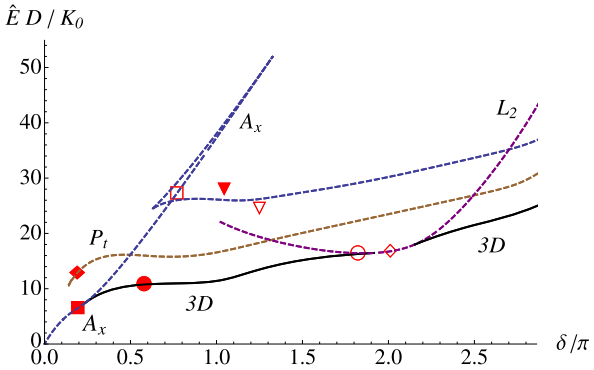

Fig. 4 Energy as function of the end-shortening δ for the post-buckling curves of Fig. 3

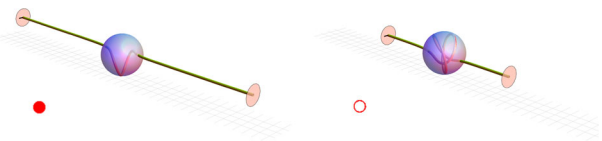

Fig. 5 3D configurations corresponding to the *filled* and *empty circles* on the post-buckling diagram of Figs. 3 and 4

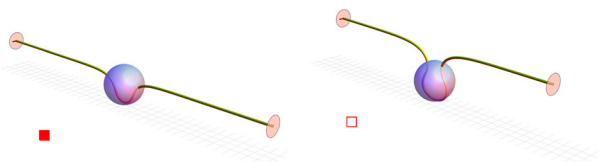

Fig. 6 2D configurations corresponding to the *filled* and *empty squares* on the post-buckling diagram of Figs. 3 and 4

decreased under a threshold value $t \simeq 3.7$, the rod buckles and the post-buckling regime first involves 2D configurations, this is the path Ax introduced in [12]. The dimensionless end-shortening δ is then gradually increased, and at $\delta \simeq 0.24\pi$ lies a pitchfork bifurcation and a secondary path, consisting of 3D configurations, emerges and progresses toward the plateau value $t_\mathrm{P} = f_\gamma - 2$ [14], see Fig. 3. Later along the path, for $\delta \simeq 1.9\pi$, another pitchfork bifurcation occurs and, for a limited δ interval, the equilibrium configurations become planar again: The 3D path merges with the path L_2, which consists in configurations which are planar and looping twice inside the sphere. After yet another pitchfork bifurcation at $\delta \simeq 2.15\pi$, the L_2 and 3D paths split again.

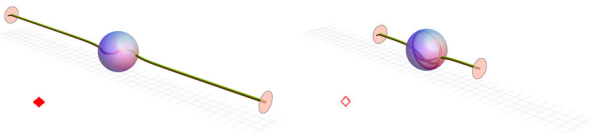

Fig. 7 2D configurations corresponding to the *filled* and *empty diamonds* on the post-buckling diagram of Figs. 3 and 4

Fig. 8 3D configurations corresponding to the *filled* and *empty triangles* on the post-buckling diagram of Figs. 3 and 4

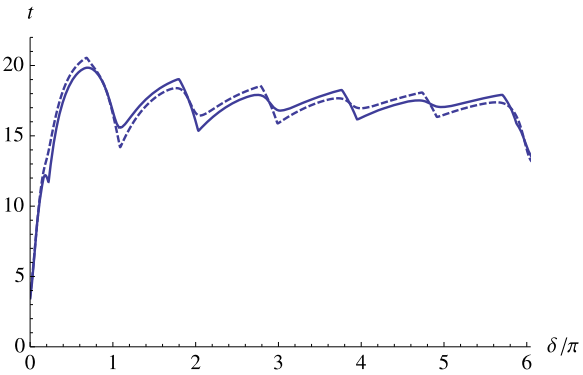

Fig. 9 Force-displacement post-buckling curves for $\ell = 20$, $f_\gamma = 20$, and either $\mathcal{R} = 0$ (*continuous line*) or $\mathcal{R} = 2\pi$ (*dashed line*). Only the succession Ax-3D-L_2-3D, which has lowest energy, is shown. For $\mathcal{R} = 0$ ($\mathcal{R} = 2\pi$), the series of events of planar-loop configurations appears around even (odd) values of δ/π

Another path, called Pt in [12], exists and is composed of configurations which are always planar. These configurations, resembling a second buckling mode, are probably unstable, but using a rod with a flat, rectangular cross-section we were able to stabilize them, see Fig. 10. No bifurcation was found along this path P_t.

In order to classify these different paths we plot the energy $\hat{E} = E_{\text{tot}} + F_\gamma(\Delta + D)$ in Fig. 4 where the lowest energy path is seen to be the succession Ax-3D-L_2-3D. Please note that yet other paths were found, but with higher energies, see, *e.g.*, the two configurations in Fig. 8. In [12] a path L_1, comprising 2D configurations which were looping once inside the sphere, was shown. This path does not fulfill the topological constraint $\mathcal{R} = 0$ and is therefore not plotted in Figs. 3 or 4. Nevertheless if the boundary condition $\mathcal{R} = 2\pi$ was used instead, such a path L_1 would come into play. We draw in Fig. 9 the post-buckling of a rod with $\ell = 20$ (and $k_3 = 0.9$, $f_\gamma = 20$, $v_0 = 2 \times 10^{-4}$, $\rho = 0.1$) and either $\mathcal{R} = 0$ or $\mathcal{R} = 2\pi$. We see that for $\mathcal{R} = 0$ ($\mathcal{R} = 2\pi$), around $\delta/\pi = 2j$ ($2j - 1$) there is an interval in which configurations with $2j$ ($2j - 1$) loops exists, with $j = 1, 2, 3, \ldots$. As the system tries to minimize the bending energy, the rod tends to wind in the sphere following the largest possible radius of curvature. This $\delta = \pi$, or $\Delta = 2\pi R$, periodicity consequently corresponds to the addition of one coil (of radius R) in the sphere: as the rod enters the attracting sphere there are periodic events where the rod adopts an ordered configuration resembling a spool. We have been able to experimentally evidence these ordered states, see Fig. 10 and [13].

6 Conclusion

In conclusion we have presented a model for the interaction of an elastic rod with a liquid drop, with the restriction that the drop remains spherical. The difference in surface energies

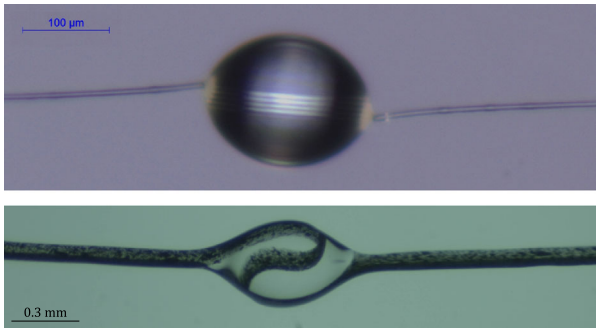

Fig. 10 (*Up*) Thermoplastic Poly Urethane (Young's modulus 17 MPa) fiber with circular cross-section (diameter 5.6 +/− 0.5 microns) spooled in a silicone oil drop (diameter $\simeq$ 200 microns, surface tension 21 mN/m) with $\mathcal{R} = 0$. There is $2\Sigma = 2.8$ mm of fiber in the drop, which corresponds to $\simeq 4.5$ spools. (*Down*) PolyVinylSiloxane beam (Young's modulus $\simeq$ 200 kPa) with rectangular cross-section (40×160 microns) bent in a silicone oil drop (diameter $\simeq 0.7$ mm) with $\mathcal{R} = 0$. The 2D configuration obtained, analogous to configurations along the P_t curve in Fig. 3, is due to the anisotropy of the cross-section which strongly favors bending in one direction

$\gamma_{SV} - \gamma_{SL}$ yields a capillary force that compresses the part of the beam which lies inside the drop. When the compression is large enough the rod buckles and coils in the drop. We have derived the rod's equilibrium equations from a variational point of view, showing that the compressive forces applied on the rod at the meniscus points were oriented toward the center of the spherical drop (Eqs. (21a), (21b)) and had their intensity depending of their orientation relative to the rod's tangent (Eqs. (24a), (24b)). We have numerically solved the equilibrium equations and found planar and spatial coiled configurations, with bifurcations between them as the end-shortening of the system is increased. More precisely we found that there is an interplay between 2D and 3D solutions, the lowest energy solution being mainly 3D with short intervals in which the rod adopts a planar-loop configuration. This intermittency scenario has still to be verified experimentally [13] but we show in Fig. 10 that solutions where the rod is tidily spooled inside the drop indeed exist.

Acknowledgements We thank Camille Dianoux and Sinan Haliyo for their help on microscopy, and Arnaud Antkowiak for comments on the variational approach. The present work was supported by ANR grant ANR-09-JCJC-0022-01, ANR-14-CE07-0023-01, and ANR-13-JS09-0009. Financial support from 'La Ville de Paris—Programme Émergence' and CNRS, through a PEPS-PTI grant, is also gratefully acknowledged.

References

1. Adda-Bedia, M., Boudaoud, A., Boué, L., Debœuf, S.: Statistical distributions in the folding of elastic structures. J. Stat. Mech. Theory Exp. **2010**(11), P11027 (2010)
2. Antman, S.S.: Nonlinear Problems of Elasticity, 2nd edn. Springer, New York (2004)
3. Arsuaga, J., Tan, R.K.Z., Vazquez, M., Sumners, D.W., Harvey, S.C.: Investigation of viral DNA packaging using molecular mechanics models. Biophys. Chem. **101–102**, 475–484 (2002)
4. Audoly, B., Pomeau, Y.: Elasticity and Geometry: From Hair Curls to the Non-linear Response of Shells. Oxford University Press, London (2010)
5. Bourgat, J.F., Le Tallec, P., Mani, S.: Modélisation et calcul des grands déplacements de tuyaux élastiques en flexion torsion. J. Méc. Théor. Appl. **7**(4), 379–408 (1988)
6. Chen, L., Yu, S., Wang, H., Xu, J., Liu, C., Chong, W.H., Chen, H.: General methodology of using oil-in-water and water-in-oil emulsions for coiling nanofilaments. J. Am. Chem. Soc. **135**(2), 835–843 (2013)

7. Cohen, A.E., Mahadevan, L.: Kinks, rings, and rackets in filamentous structures. Proc. Natl. Acad. Sci. USA **100**(21), 12141–12146 (2003)
8. de Gennes, P.G., Brochard-Wyard, F., Quere, D.: Capillarity and Wetting Phenomena: Drops, Bubbles, Pearls, Waves. Springer, New York (2003)
9. Doedel, E., Keller, H.B., Kernevez, J.P.: Numerical analysis and control of bifurcation problems (I): bifurcation in finite dimensions. Int. J. Bifurc. Chaos Appl. Sci. Eng. **1**(3), 493–520 (1991)
10. Domokos, G., Healey, T.: Hidden symmetry of global solutions in twisted elastic rings. J. Nonlinear Sci. **11**, 47–67 (2001)
11. Duprat, C., Protiere, S., Beebe, A.Y., Stone, H.A.: Wetting of flexible fibre arrays. Nature **482**(7386), 510–513 (2012)
12. Elettro, H., Vollrath, F., Antkowiak, A., Neukirch, S.: Coiling of an elastic beam inside a disk: a model for spider-capture silk. Int. J. Non-Linear Mech. **75**, 59–66 (2015)
13. Elettro, H., Neukirch, S., Antkowiak, A.: Negative stiffness regimes and coiling morphology signatures in drop-on-coilable-fiber systems (2016). In preparation
14. Elettro, H., Neukirch, S., Vollrath, F., Antkowiak, A.: In-drop capillary spooling of spider capture thread inspires hybrid fibers with mixed solid–liquid mechanical properties. Proc. Natl. Acad. Sci. USA **113**(22), 6143–6147 (2016)
15. Fargette, A., Neukirch, S., Antkowiak, A.: Elastocapillary snapping: capillarity induces snap-through instabilities in small elastic beams. Phys. Rev. Lett. **112**(13), 137802 (2014)
16. Katzav, E., Adda-Bedia, M., Boudaoud, A.: A statistical approach to close packing of elastic rods and to DNA packaging in viral capsids. Proc. Natl. Acad. Sci. USA **103**(50), 18900–18904 (2006)
17. Kehrbaum, S., Maddocks, J.H.: Elastic rods, rigid bodies, quaternions and the last quadrature. Philos. Trans. R. Soc. Lond. Ser. A, Math. Phys. Sci. **355**(1732), 2117–2136 (1997)
18. LaMarque, J.C., Le, T.V., Harvey, S.C.: Packaging double-helical DNA into viral capsids. Biopolymers **73**(3), 348–355 (2004)
19. Leforestier, A., Livolant, F.: Structure of toroidal DNA collapsed inside the phage capsid. Proc. Natl. Acad. Sci. USA **106**(23), 9157–9162 (2009)
20. Lorenceau, É., Clanet, C., Quéré, D.: Capturing drops with a thin fiber. J. Colloid Interface Sci. **279**(1), 192–197 (2004)
21. Martel, R., Shea, H.R., Avouris, P.: Rings of single-walled carbon nanotubes. Nature **398**(6725), 299 (1999)
22. Neukirch, S., Henderson, M.E.: Classification of the spatial clamped elastica: symmetries and zoology of solutions. J. Elast. **68**, 95–121 (2002)
23. Neukirch, S., Roman, B., de Gaudemaris, B., Bico, J.: Piercing a liquid surface with an elastic rod: buckling under capillary forces. J. Mech. Phys. Solids **55**(6), 1212–1235 (2007)
24. Py, C., Reverdy, P., Doppler, L., Bico, J., Roman, B., Baroud, C.N.: Capillary origami: spontaneous wrapping of a droplet with an elastic sheet. Phys. Rev. Lett. **98**(15), 156103 (2007)
25. Roman, B., Bico, J.: Elasto-capillarity: deforming an elastic structure with a liquid droplet. Phys. Condens. Matter **22**(49), 493101 (2010)
26. Steigmann, D.J., Faulkner, M.G.: Variational theory for spatial rods. J. Elast. **33**(1), 1–26 (1993)
27. Stoop, N., Najafi, J., Wittel, F.K., Habibi, M., Herrmann, H.J.: Packing of elastic wires in spherical cavities. Phys. Rev. Lett. **106**, 214102 (2011)
28. van der Heijden, G.H.M., Peletier, M.A., Planqué, R.: On end rotation for open rods undergoing large deformations. Q. Appl. Math. **65**(2), 385–402 (2007)
29. Vetter, R., Wittel, F., Stoop, N., Herrmann, H.: Finite element simulation of dense wire packings. Eur. J. Mech. A, Solids **37**, 160–171 (2013)
30. Vollrath, F., Edmonds, D.T.: Modulation of the mechanical properties of spider silk by coating with water. Nature **340**, 305–307 (1989)